Supplementary Information

Identification and quantification of multinuclear Cu active sites derived from monomeric Cu moieties for dry NO oxidation over Cu-SSZ-13

Ishant Khurana[1,*], Jonatan D. Albarracin-Caballero[1], Arthur J. Shih[1,2,*]

[1]Davidson School of Chemical Engineering, Purdue University, West Lafayette, IN 47907, USA
[2]Current address: Department of Materials Science and Engineering, Northwestern University, Evanston, Illinois 60208, USA

*Corresponding authors: E-mail: ikhuran@purdue.edu (I. Khurana), arthur.shih@northwestern.edu (A. J. Shih)

Table of Contents

Section S1: Detailed Experimental Procedures

Synthesis of SSZ-13

High-aluminum SSZ-13 zeolites (Si:Al = 4.5) were synthesized as previously reported by Fickel et al. [1], which is based on a patent by Zones [2]. A molar ratio of 1 SiO_2, 0.031 Al_2O_3, 0.017 TMAdaOH, 0.770 Na_2O, 12.1 H_2O was used in the synthesis solution. Briefly, a 1 M NaOH solution (3.3 wt% NaOH, Alfa Aesar) was added to deionized water (18.2 cm·MΩ) in a perfluoroalkoxy alkane (PFA) jar and stirred for 15 minutes. Next, sodium silicate (10.6 wt % Na_2O, 25.6 wt% SiO_2, Sigma Aldrich) was added to the NaOH solution and stirred for 15 minutes. Then, NH_4-Y zeolite (Zeolyst CBV300, Si:Al = 2.6) was added and the mixture was stirred for 30 minutes. Finally, an aqueous TMAdaOH solution (25 wt%, Sachem) was added to the mixture and stirred for 30 minutes, all under ambient conditions. ~30 mL of the synthesis mixture was then transferred to each 45 mL Teflon-lined stainless steel autoclaves (Parr Instruments) and rotated at 60 RPM for 6 days in a forced convection oven (Yamato DKN-402C) at 413 K.

Low aluminum SSZ-13 zeolites (Si:Al 15 to 25) were synthesized in hydroxide media using a previously reported procedure by Deka et al. [3]. A molar ratio of 1 SiO_2, 0.0167 to 0.033 Al_2O_3, 0.25 TMAdaOH, 0.125 Na_2O, 44 H_2O was used to obtain Na^+:$TMAda^+$ = 1 and Si:Al = 15 or 25 in the synthesis solution. A typical synthesis involved adding an aqueous TMAdaOH solution to deionized H_2O in a PFA jar and stirring the solution for 15 minutes. Next, aluminum hydroxide was added to the aqueous TMAdaOH solution. Then, a 5M NaOH solution (16.7 wt% NaOH in deionized water; NaOH pellets 98 wt%, Alfa Aesar) was added dropwise to the solution and stirred for 15 minutes. Finally, colloidal silica was added and the mixture was stirred for 2 h under ambient conditions. All synthesis reagents were used without further purification. The synthesis solution was then transferred to a 45 mL Teflon-lined stainless-steel autoclave and placed in a forced convection oven at 433 K and rotated at 40 RPM for 6 days.

After crystallization, the stainless steel autoclaves were removed from the oven and immediately quenched via submersion in cold water directly from the tap for at least several hours. The crystallized zeolite was separated from the liquid via centrifugation and washed copiously with alternating cycles of acetone and water until the water pH decreased to between 7 and 8. The zeolite was then dried in air in an 80°C oven. Once dry, the zeolite, which still has the structural directing agent (TMAdaOH) in its pores, was crushed in a mortar and pestle to increase its surface area, ~5 to 10 g were loaded into a vertical quartz tube between two plugs of quartz wool (CGQ-0690-02, 8-15 microns coarse porosity, ChemGlass), and calcined under ~100 sccm of dry air (AirZero, < 1 ppm total hydrocarbons, Indiana Oxygen Co.) at 873 K (ramp from 298K to 873 K with a ramp rate of 2 K min^{-1}, held at 873 K for 8 hours, then cooled to room temperature). A pressure gauge upstream of the reactor was used to ensure that the pressure drop from the finely packed bed did not exceed 5 psig. The final product is Na-SSZ-13, where the anionic sites in the zeolite are protected by sodium cations.

Ion-exchange between Na^+ and NH_4^+ was performed by stirring 1 g Na-SSZ-13 per 100 g 0.1 M NH_4NO_3 (>99%, Sigma-Aldrich, dissolved in deionized water) at 353 K for 10 h. The resulting NH_4-SSZ-13 was washed 3 times with 50 mL of water per gram zeolite then dried at 373 K for > 24 hours under ambient air. The resulting zeolite was then crushed with a mortar pestle and calcined in the same furnace from the previous paragraph under ~100 sccm of dry air (AirZero, Indiana Oxygen) at 823 K (ramp from 298K to 873 K with a ramp rate of 2 K min^{-1}, held at 823 K for 8 hours, then cooled to room temperature). This calcination desorbed the NH_3 and resulted in H-SSZ-13.

Aqueous-phase copper ion-exchange of H-SSZ-13

Cu-zeolites were prepared by aqueous-phase Cu ion exchange of H-form zeolites with a $Cu(NO_3)_2$ solution (0.001M to 0.1M, with higher concentrations resulting in higher Cu loadings, 100 $cm^3_{solution}\ g_{catalyst}^{-1}$; 99.999 wt% $Cu(NO_3)_2$ from Sigma Aldrich) for 4 h and 300 RPM at ambient conditions, during which the pH was controlled to 4.9 ± 0.1 through dropwise addition of a 1.0 M NH_4OH solution (Sigma Aldrich, 28.0% ammonium hydroxide solution, ACS reagent grade) to increase the extent of Cu exchange. Care was taken to ensure that solid hydroxide precipitates do not form during the Cu ion exchange process as they lead to clustered Cu_xO_y [4]. Cu-exchanged SSZ-13 was recovered by centrifugation and washed with deionized water six times (70 ml g $catalyst^{-1}$ per wash). Cu-SSZ-13 catalysts were further dried at 373 K in ambient air in a free convention oven for 12 hours, crushed in a mortar and pestle, then calcined in dry air (AirZero, < 1ppm total hydrocarbons, Indiana Oxygen Co.) to 773 K at a rate of 1 K min^{-1}.

Atomic Absorption Spectroscopy (AAS) to determine elemental composition

~0.03 g of dry sample (H-SSZ-13 or Cu-SSZ-13) were dissolved in ~2 mL of hydrofluoric acid (HF) (Mallinckrodt Baker, 48% HF, Baker Analyzed® A.C.S. Reagent) in a 60 mL high density polyethylene (HDPE) bottle (2 oz., 60 mL Nalgene™ Wide-Mouth Amber HDPE bottle). A polyethylene pipet was used to transfer the HF. The sample was capped and left to dissolve for 12 hours then diluted with approximately 50 mL of deionized water (Millipore, 18.2 cm·MΩ resistivity at 298 K). Bulk elemental composition was determined using atomic absorption spectroscopy (AAS) on a Perkin Elmer AAnalyst 300. Silicon AAS standards were created by diluting a 1000 ppm silicon AAS standard solution (Sigma Aldrich, TraceCERT®, 1000 mg/L Si in NaOH) to 15, 75, and 150 ppm. A linear calibration curve (ppm_{Si} versus Si absorbance at 251.6 nm) was determined by plotting the absorbance of each silicon standard at 251.6 nm. Analogous procedures were used for aluminum and copper on all reported SSZ-13 catalysts. Results are presented in Table S1.

Cu site characterization and quantification

Monomeric Z_2Cu and ZCuOH sites on each Cu-SSZ-13 zeolite were quantified after oxidative treatment (20% O_2, 773 K) by quantifying the number of residual protons (H^+) that remained after Cu exchange, given that Z_2Cu sites exchange with two protons and ZCuOH sites exchange

with one proton. The quantification was performed using methods that selectively titrate residual H^+ sites in small-pore, metal-exchanged zeolites [5–7]. The titration method involves saturation of zeolites (~0.03 to 0.05 g) with NH_3 at 433 K (500 ppm, balance He, 2 h, 350 mL min^{-1}), followed by removal of physisorbed and Cu-bound NH_3 by treatment in wet helium (2.5-3.0% H_2O in balance He, 8 h, 350 mL min^{-1}), to selectively retain surface NH_4^+ species [5,6]. NH_3 was then evolved in a subsequent temperature programmed desorption (TPD) in He (350 mL min^{-1}) to 823 K (0.083 K s^{-1}), and quantified using on-board calibrations in a MKS Multigas 2030 gas-phase FT-IR spectrometer.

Co^{2+} ion exchange was used to quantify the fraction of total Al present as Al pairs by titrating the number of paired Al to saturation [8]. Co-SSZ-13 zeolites were prepared by ion exchange of H-SSZ-13 with an aqueous 0.25M $Co(II)(NO_3)_2$ solution (150 ml g $catalyst^{-1}$) for 4 h at ambient conditions, not controlling the pH (pH stabilized between 3.2-3.6 after 4 h). Data also presented in Table S1.

Steady state NO oxidation kinetic measurements

NO oxidation kinetics (rates, reaction orders, and apparent activation energies) were measured with a down-flow tubular quartz reactor with an inner diameter of 13 mm and an overall length of 400 mm. A coarse quartz frit was installed at the midpoint of the reactor, over which a layer of quartz wool was placed and flattened. All samples were pelletized (Specac 13mm Diameter Stainless Steel Evaluable Pellet Die) under 10,000 psi pressure (Carver Laboratory Press), ground using a mortar and pestle, then sieved to retain 125 to 250 μm particles (W.S. TYLER No. 60 and No. 120 all-stainless-steel sieves) to minimize the pressure drop of the flow of gas across the powder catalyst bed. Typically, ~0.015 to 0.050 g of sieved Cu-SSZ-13 catalyst was mixed with enough inert silica gel (Fisher Chemical Silica Gel (Davisil) Sorbent, Grade 923) to obtain a bed height of ~5 mm. Another layer of quartz wool was pressed slightly over the top of the catalyst bed to ensure uniformity of the bed. The temperature across the catalyst bed was measured by placing two K-type thermocouples, one touching the quartz wool above the catalyst bed and the other ~2 mm below the glass frit. Aluminum foil was wrapped around the quartz reactor to an outer diameter of ~2.54 cm to enhance heat conduction and minimize radial and axial temperature gradients within the bed [9]. The reactor was then secured within a clamshell furnace (Applied Test Systems) and leak checked by pressurizing with helium (99.999%, ultra high purity, Indiana Oxygen Co.) to 5 psig and held for 20 minutes. The standard NO oxidation feed consisted of 300 ppm NO (diluted from 3.5% NO/Ar, standard grade, Praxair Distribution, Inc.), 150 ppm NO_2 (diluted from 1.0% NO_2/Ar, standard grade, Praxair Distribution Inc.), 10% O_2 (diluted from 99.5% O2, commercial grade, Indiana Oxygen Co.) in balance N_2 (boiloff from liquid Nitrogen, Linde). The feed gases from the gas manifold were preheated by flowing through a preheater (maintained at 300 °C) prior to entering the main reactor to further minimize axial gradients as measured using the two thermocouples (typically < 5 K difference). Gas-phase concentrations of NO, NO_2, CO_2, H_2O, and N_2O were meausred using a Fourier transform infrared (FTIR) analyzer (MKS Multigas™ 2030 gas-phase FTIR spectrometer). The FTIR analyzer had a spectral resolution of 0.5 cm^{-1}, and factory supplied calibrations were used to quantify the various gas concentrations.

The conversion of NO was measured according to Equation 1, where NO_{in} and NO_{out} are the concentrations of NO entering and leaving the reactor in ppm.

$$NO\ conversion = \frac{NO_{in} - NO_{out}}{NO_{in}} \cdot 100 \qquad \text{(Equation 1)}$$

In the limit of differential conversion (< ~20%) with product (i.e. NO_2) co-fed, the gas concentrations (NO, O_2, NO_2) and catalyst bed temperature can be assumed constant [9–14], resulting in systematic errors ranging from near zero (< 5% conversion) to 1.2% (20% conversion) [10], much lower than the error from experimental repeats (typically 10 to 20%). This allows the NO consumption rate to be calculated using the continuous stirred tank reactor (CSTR) design equation:

$$-r_{overall}(mol\ NO\ mol\ Cu^{-1}s^{-1}) = \frac{NO\ conversion}{1000000 * mol\ Cu} \cdot NO_{in} \cdot \dot{V}_{total} \cdot \frac{P}{RT} \qquad \text{(Equation 2)}$$

where NO_{in} is the inlet NO concentration in ppm, $\dot{V}_{total}$ is the total volumetric flow rate, P is 1 atm, T is ambient temperature, and R is the gas constant. All reaction rates and kinetic parameters reported were collected in the limit of differential conversion and with products co-fed.

Based on the overall NO oxidation rate ($r_{overall}$), the normalized forward rates (r_{fwd}) were reported in the form of a power rate law model. The approach to equilibrium (β) was included because the NO oxidation rates could potentially be limited by equilibrium under the relevant reaction temperatures [55].

$$r_{fwd} = r_{overall}(1 - \beta) \qquad \text{(Equation 3)}$$

$$r_{fwd} = Ae^{\frac{-E_A}{RT}}[NO]^a[O_2]^b[NO_2]^c \qquad \text{(Equation 4)}$$

$$\beta = \frac{[NO_2]}{K[NO]^2[O_2]} \qquad \text{(Equation 5)}$$

With K as the equilibrium constant for the NO oxidation reaction, the value of β for all the measurements were less than 0.18, indicating that the reaction rates measured were sufficiently far from equilibrium. A is the pre-exponential factor (s^{-1}) and E_A the activation energy (kJ mol^{-1}). a, b, and c represent forward reaction orders with respect to NO, O_2 and NO_2 respectively. The nitrogen balance in and out of the reactor was quantitatively confirmed to be complete within less than 5% for all measurements using $(NO + NO_2)_{in} - (NO + NO_2)_{out}$.

Carbon Monoxide Temperature Programmed Reduction (CO-TPR)

Carbon monoxide temperature programmed reduction (CO-TPR) was performed following procedures outlined in Beutel et al., Lee et al., and Da Costa et al. [15–17]. The sample (~30 mg, sieved to 125 to 250 µm) was loaded into an AutoChem™II 2920 equipped with a mass spectrometer. The sample was first heated to 773 K at a rate of 9 K min^{-1} under the flow of 50 mL min^{-1} dry air (commercial grade, Indiana Oxygen Co.) and held for 2 hours before cooling to room temperature. The sample was then flushed with 50 mL min^{-1} He (Ultra high purity, Indiana

Oxygen) at room temperature for 2 hours to flush out residual oxygen. CO-TPR was then performed under 18 mL min^{-1} flow of 5% CO/He (standard grade, Praxair Distribution, Inc.) up to the temperature of 833 K with a ramp rate of 10 K min^{-1}. CO2 evolution was probed using the m/z = 44 signal in the mass spectrometer. The total CO_2 evolved was quantified by integrating the CO-TPR between 303 K and 573 K.

Fourier-Transform Infrared Spectroscopy (FTIR)

In-situ transmission FTIR was collected on zeolite samples using a Nicolet 6700 FTIR spectrometer equipped with a liquid nitrogen-cooled mercury cadmium telluride (MCT) detector. Catalyst samples (~40 to 50 mg) were pressed into a self-supporting wafer (~2 cm in diameter) and placed in a custom-built FTIR cell [18,19]. Wafers were treated in flowing oxygen (10% O_2/He, standard grade, Praxair Distribution, Inc.) to 673 K for 30 min and then cooled to 575 K, prior to the exposure to NO oxidation reaction gases 300 ppm NO (diluted from 0.5% NO/He, Praxair Distribution, Inc.), 150 ppm NO_2 (diluted from 1% NO_2/He, Praxair Distribution, Inc.), 10% O_2 (diluted from 99.999%, ultra high purity, Matheson Tri-Gas), in balance He (99.999%, ultra high purity, Matheson Tri-Gas). Spectra were collected with a resolution of 4 cm^{-1}, averaged over 36 scans and baseline corrected.

Section S2: Characterization and Kinetics of Cu-SSZ-13

Table S1. Bulk elemental analysis and fraction of monomeric Cu^{II} and $Cu^{II}(OH)$ sites on a series of Cu-exchanged SSZ-13 samples with varying Si:Al (4.5 - 25) and Cu:Al (0.03 - 0.44)

Si/Al[a]	Cu wt %[a]	Cu:Al[a]	H^+:Al[b]	Excess H^+:Al[b]	Co:Al[c]	Micropore Volume[d]	$Cu^{II}OH$:Al[e]	Cu^{II}:Al[e]
4.5	0.0	0.00	0.65	-	0.19	0.26	0.00	0.00
	1.7	0.08	0.42	0.05	-	-	0.00	0.08
15	0.0	0.00	0.98	-	0.10	0.18	0.00	0.00
	0.2	0.03	0.93	0.03	-	-	0.00	0.03
	0.8	0.12	0.73	0.09	-	-	0.03	0.09
	1.6	0.24[f]	0.80	0.00	-	-	0.24	0.00
	1.7	0.25	0.64	0.10	-	-	0.16	0.09
	2.4	0.37	0.58	0.08	-	-	0.28	0.09
	2.8	0.42	0.50	0.08	-	-	0.33	0.09
	2.9	0.44	0.51	0.09	-	-	0.35	0.09
25	0.0	0.00	0.98	-	0.05	0.20	0.00	0.00
	1.1	0.30	0.67	0.04	-	-	0.26	0.04
	1.6	0.42	0.58	0.04	-	-	0.38	0.04

[a]Atomic composition determined using Atomic Absorption Spectroscopy
Errors are Si:Al = ± 1 and Cu:Al = ± 0.03
[b]Residual Brønsted acid sites counted in oxidized and reduced form using NH_3 titration method described in [5]
[c]Paired Al sites counted using amount of Co titrated following the procedure described in [8].
[d]Micropore volume from Ar adsorption isotherms.
Error is ± 0.01 $cm^3\ g^{-1}$
[e]Determined from titration of residual H^+ sites by NH_3 and thermodynamic preferences for Cu^{II} and $Cu^{II}OH$ siting [5] and [6]
[f]Sample synthesized with all framework Al as isolated Al and 100% of the Cu is exchanged as [Cu-OH]

Section S3: NO Oxidation Kinetics

Table S2. Summary of NO oxidation kinetic data on a series of Cu-exchanged SSZ-13 samples with varying Si:Al (4.5-25) and Cu:Al (0.03-0.44)

Cu:Al	$Cu^{II}OH$:Al	CuOH density (mol m^{-3})	Eapp[a] (kJ mol^{-1})	Rate [b] (10^{-4} mol NO mol Cu^{-1} s^{-1})	NO order[a]	NO_2 order[a]	O_2 order[a]
			SSZ-13 Si:Al = 4.5				
0.00	0.00	0.00	n.d.	0.0	n.d.	n.d.	n.d.
0.08	0.00	0.00	n.d.	0.0	n.d.	n.d.	n.d.
0.20	0.00	0.00	n.d.	0.0	n.d.	n.d.	n.d.
0.31*	0.00	0.00	45	0.6	1.5	-0.8	0.9
0.35*	0.00	0.00	51	1.4	1.4	-0.7	0.8
0.39*	0.00	0.00	53	1.5	1.5	-0.8	0.8
1.60*	0.00	0.00	55	1.7	1.6	-0.9	0.9
			SSZ-13 Si:Al = 15				
0.00	0.00	0.00	n.d.	0.0	n.d.	n.d.	n.d.
0.03	0.00	0	n.d.	0.0	n.d.	n.d.	n.d.
0.12	0.03	47	n.d.	0.0	n.d.	n.d.	n.d.
0.24[c]	0.24	375	48	0.5	0.9	-0.9	0.7
0.25	0.16	251	46	0.7	1.4	-0.6	0.7
0.37	0.28	439	56	0.9	1.4	-0.6	0.7
0.42	0.33	517	65	1.2	1.4	-0.8	0.7
0.44	0.35	548	55	1.3	1.3	-0.6	0.7
			SSZ-13 Si:Al =25				
0.00	0.00	0.00	n.d.	0.0	n.d.	n.d.	n.d.
0.30	0.25	251	61	0.8	1.5	-0.8	0.9
0.42	0.37	366	67	1.0	1.3	-1.0	0.8

[a] Measured at 573 K. Error in activation energy ± 7 kJ mol^{-1} and orders ± 0.1 (NO_2 and O_2) and ± 0.2 (NO)
[b] Measured under NO oxidation conditions of 300 ppm NO, 150 ppm NO_2, 10% O_2 and 550 K
[c] Sample synthesized with isolated Al on the SSZ-13 framework 100% of the Cu is exchanged as $[Cu\text{-}OH]^+$
*From Verma et al. [20]
n.d. = did not display detectable NO oxidation rate (< 0.3×10^{-4} mol_{NO} mol_{Cu}^{-1} s^{-1}).

Table S3. CO TPR (carbon monoxide temperature programmed reduction) results.

Si:Al	Cu wt %	Cu:Al	$Cu^{II}OH$:Al	CO_2:Cu_{total}	CO_2:$[Cu\text{-}OH]^+$
4.5	1.7	0.08	0.00	0.00	0.00
15	0.8	0.12	0.03	0.00	0.00
	1.7	0.25	0.16	0.24	0.38
	2.4	0.37	0.28	0.34	0.45
	2.8	0.42	0.33	0.41	0.52
	2.9	0.44	0.35	0.40	0.50
25	1.1	0.30	0.26	0.29	0.33
	1.6	0.42	0.38	0.38	0.42

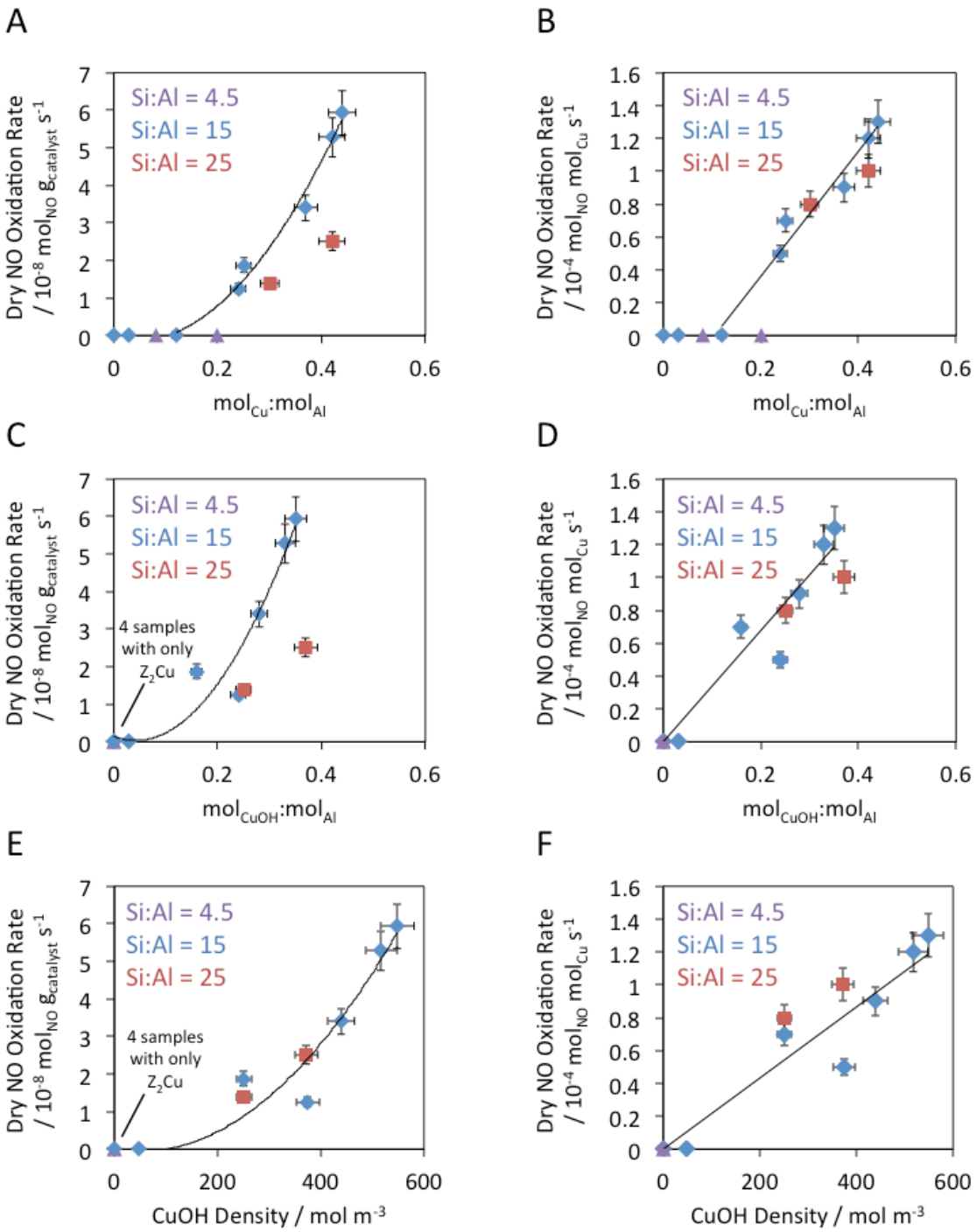

Figure S1. (A) Dry NO oxidation rate normalized per gram catalyst plotted versus the Cu:Al molar ratio. (B) Dry NO oxidation rate normalized per mol Cu plotted versus the Cu:Al molar ratio. (C) Dry NO oxidation rate normalized per gram catalyst plotted versus the CuOH:Al molar ratio. (D) Dry NO oxidation rate normalized per mol Cu plotted versus the CuOH:Al molar ratio. (E) Dry NO oxidation rate normalized per gram catalyst plotted versus the CuOH density. (F) Dry NO oxidation rate normalized per mol Cu plotted versus the CuOH density.

Section S4: Spectroscopic Response of Cu dimers to NO Oxidation

Diffuse reflectance UV-Visible spectra were recorded under various gas conditions using a Varian UV-Visible-NIR spectrophotometer (Cary 5000) with a diffuse reflectance accessory consisting of two ellipsoidal mirrors (Harrick Scientific Praying Mantis). Barium sulfate ($BaSO_4$, 99.9%, Sigma-Aldrich) was used as the 100% reflectance standard. An *in-situ* sample holder was loaded with approximately 0.1 g of sieved sample (pelleted and sieved to retain particles between 125-250 µm in diameter). Spectra were collected from 7000 to 50000 cm^{-1} with a scan speed of 2000 cm^{-1} min^{-1} using the following two conditions.

Condition 1: Sample was dehydrated at 673 K in oxidizing atmosphere of dry air (Commercial grade, Indiana Oxygen) (total flow of 50 ml min^{-1}) and held for 2 hrs. Sample was then cooled down to 473 K under the same oxidizing atmosphere. Spectra was then collected at 473 K.

Condition 2: Sample was exposed to NO oxidation reaction conditions i.e. 150 ppm NO, 150 ppm NO_2 and 10% O_2 at 575 K (total flow of 50 ml min^{-1}) and held for 2 hrs. Sample was then cooled down to 473 K under the same gas condition. Spectra was then collected at 473 K.

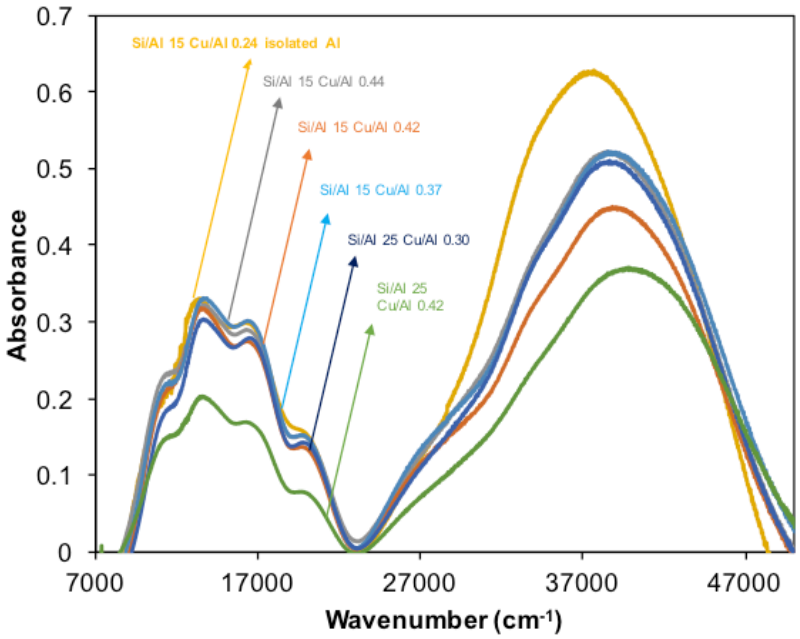

Figure S2. Diffuse Reflectance UV-visible spectra spectra at 473 K of Cu-SSZ-13 Si:Al = 15 Cu:Al = 0.12 - 0.44, and Si:Al = 25, Cu:Al = 0.30 - 0.42 samples after high temperature oxidative treatment (20% O2 at 673 K)

Diffusive Reflectance UV-visible spectra of Cu-SSZ-13 samples after high temperature oxidative treatment showed multiple absorption bands at 10900 cm^{-1}, 13600 cm^{-1}, 16500 cm^{-1} and 19700 cm^{-1} corresponding to d-d transitions of d^9 Cu(II) state as well as shoulders at 28200 cm^{-1} and 34800 cm^{-1}

representative of Ligand to Metal Charge Transfer (LMCT) electronic transitions (Figure S3). Features at 16500 cm^{-1} and 19700 cm^{-1} have been previously assigned to $\{Cu(II)–O_2–Cu(II)\}^{2+}$ (trans-μ-1,2-peroxo dicopper(II)) [21]. The broad band with maximum intensity at 28200 cm^{-1} in Figure 3 was interpreted as a peroxo to Cu(II) charge transfer band for $\{Cu(II)–O_2–Cu(II)\}^{2+}$ (trans-μ-1,2-peroxo dicopper(II)) [21]. On the other hand, the absorption shoulder at 34800 cm^{-1} was ascribed to $\{Cu(II)–O–Cu(II)\}^{2+}$ (mono–(μ–oxo) dicopper(II)) [21].

In-situ UV-vis spectra collected under NO oxidation reaction conditions provides additional evidence that these dimeric Cu sites are the active site for NO oxidation (Figure S2). Upon admission of NO and O_2, decrease of absorption peak intensities at 16500 cm^{-1} and 19700 cm^{-1}, ascribed to $\{Cu(II)–O_2–Cu(II)\}^{2+}$ (trans-μ-1,2-peroxo dicopper(II)), indicate that the NO oxidation reactive species is likely $\{Cu(II)–O_2–Cu(II)\}^{2+}$ and/or $\{Cu(II)–O–Cu(II)\}^{2+}$ [22].

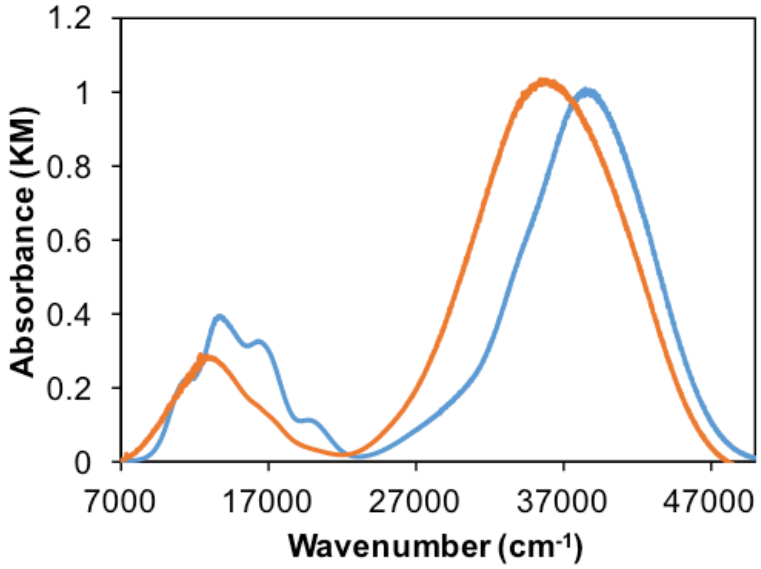

Figure S3. Diffuse Reflectance UV-visible spectra at 250°C of Cu-SSZ-13 Si:Al 15 Cu:Al 0.44 after high temperature oxidative treatment (20% O_2 at 673 K) (blue) and under NO oxidation reaction conditions (300 ppm NO, 150 ppm NO_2 and 10% O_2 in balance He) (orange)

Section S5: Determining Turnover Rates of the Three Cu-oxo Pools

Table S4. Compilation of all TOR initial guesses tested and the resulting converged TORs and after minimizing the sum of the absolute value of the residuals ($\Sigma|\Delta TOR_x|$).

Initial Guess / s^{-1}			Converged / s^{-1}			Sum of residuals	
TOR_1	TOR_2	TOR_3	TOR_1	TOR_2	TOR_3	$\Sigma\|\Delta TOR_x\|$ / s^{-1}	Comments
0	0	0	3.97	2.54	2.25	0.24	Local minima
1	1	1	3.97	2.54	2.25	0.24	Local minima
2	2	2	3.97	2.54	2.25	0.24	Local minima
3	3	3	5.73	3.58	0.19	0.12	Local minima
4	4	4	5.87	4.56	-1.19	0.19	Negative TOR not physical
5	5	5	3.97	2.54	2.25	0.24	Local minima
6	6	6	5.87	4.56	-1.19	0.19	Negative TOR not physical
7	7	7	5.87	4.56	-1.19	0.19	Negative TOR not physical
2	3	4	5.87	4.56	-1.19	0.19	Negative TOR not physical
2	4	3	5.87	4.56	-1.19	0.19	Negative TOR not physical
3	2	4	5.56	2.35	1.91	0.23	Local minima
3	4	2	5.87	4.56	-1.19	0.19	Negative TOR not physical
4	3	2	5.73	3.58	0.19	0.12	Local minima
4	2	3	3.97	2.54	2.25	0.24	Local minima

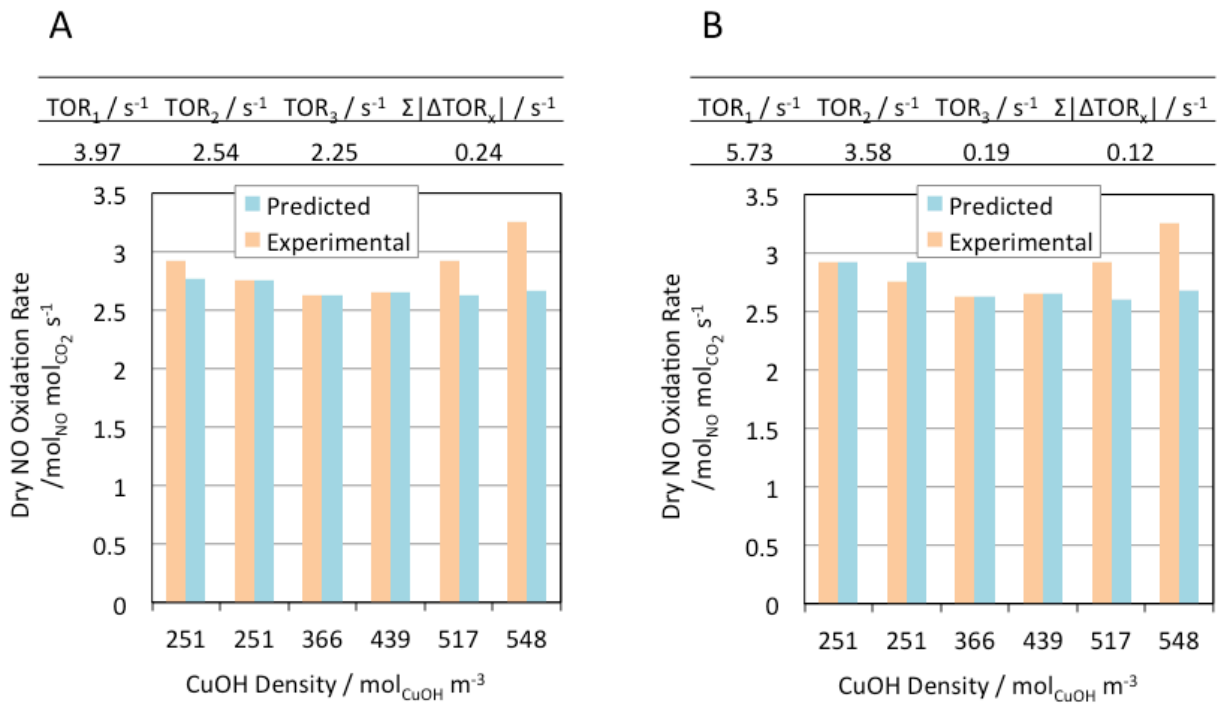

Figure S4. Comparisons between the predicted (turquoise) and predicted (orange) dry NO oxidation rates for the two local minima discovered.

Section S6: NO Oxidation Rate Law Analysis

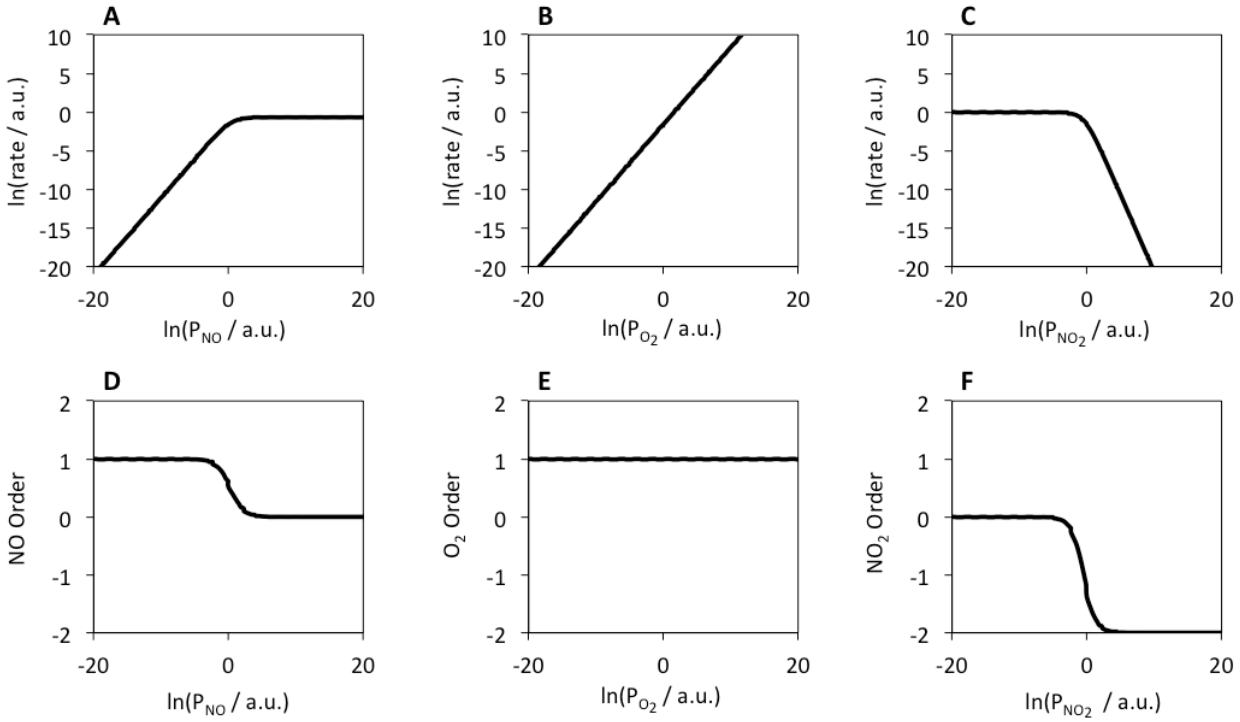

Figure S5. Effect of the (A) NO pressure, (B) O_2 pressure, and (C) NO_2 pressure on the NO oxidation rate and the NO, O_2, and NO_2 reaction orders (D, E, F, respectively) where the first elementary step of Scheme 1 is rate limiting. The NO order decreases from 1 to 0 with increasing NO pressure. The O_2 order stays at 1, independent of the O_2 pressure. The NO_2 order decreases from 0 to -2 with increasing NO_2 pressure.

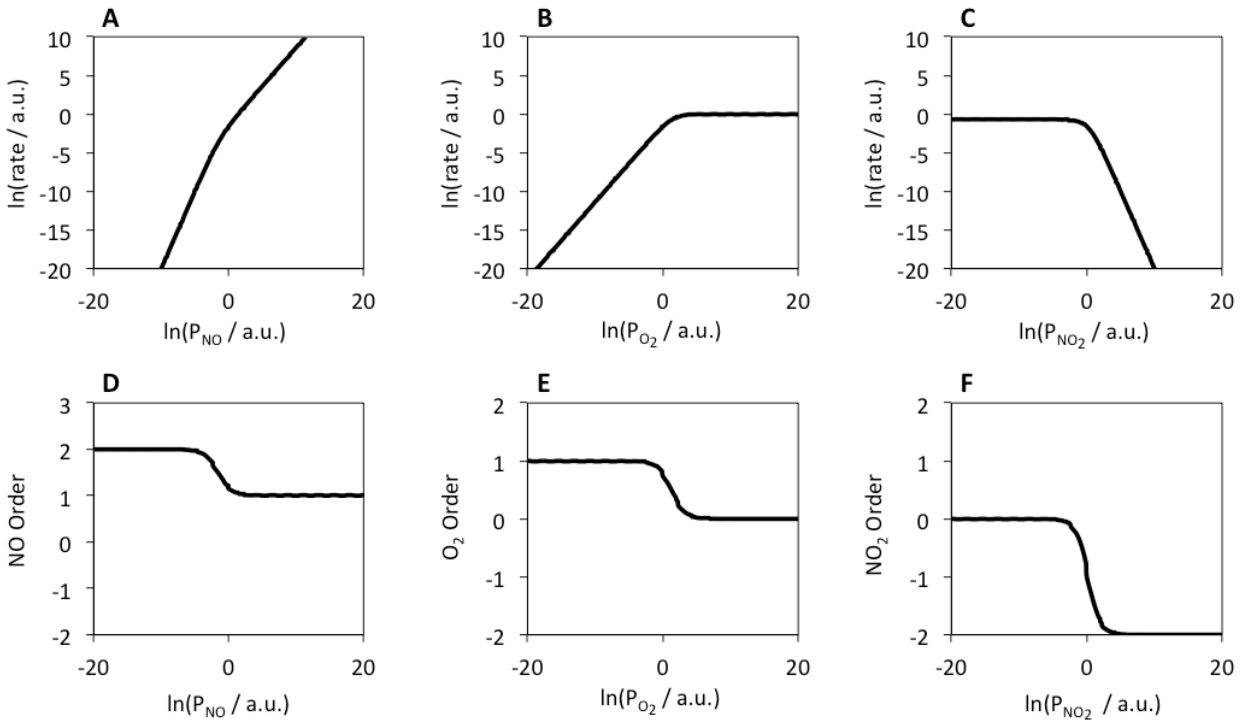

Figure S6. Effect of the (A) NO pressure, (B) O_2 pressure, and (C) NO_2 pressure on the NO oxidation rate and the NO, O_2, and NO_2 reaction orders (D, E, F, respectively) where the second elementary step of Scheme 1 is rate limiting. The NO order decreases from 2 to 1 with increasing NO pressure. The O_2 order decreases from 1 to 0 with increasing O_2 pressure. The NO_2 order decreases from 0 to -2 with increasing NO_2 pressure.

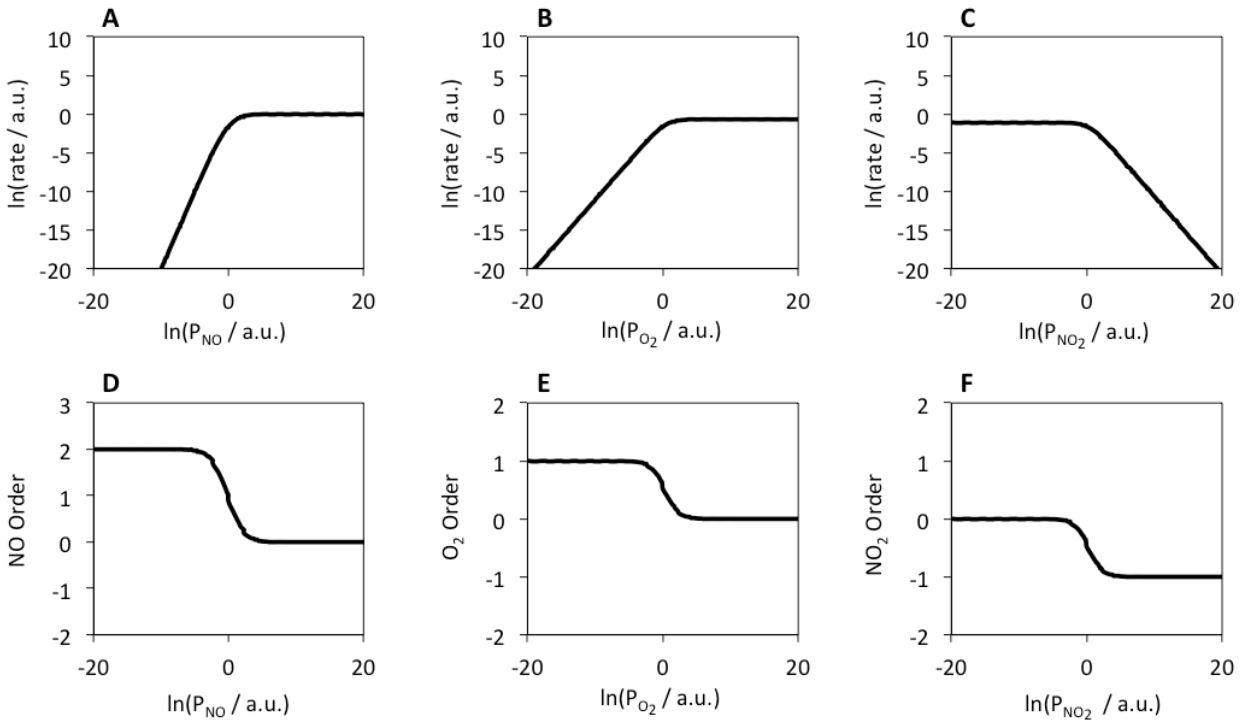

Figure S7. Effect of the (A) NO pressure, (B) O_2 pressure, and (C) NO_2 pressure on the NO oxidation rate and the NO, O_2, and NO_2 reaction orders (D, E, F, respectively) where the third elementary step of Scheme 1 is rate limiting. The NO order decreases from 2 to 0 with increasing NO pressure. The O_2 order decreases from 1 to 0 with increasing O_2 pressure. The NO_2 order decreases from 0 to -1 with increasing NO_2 pressure.

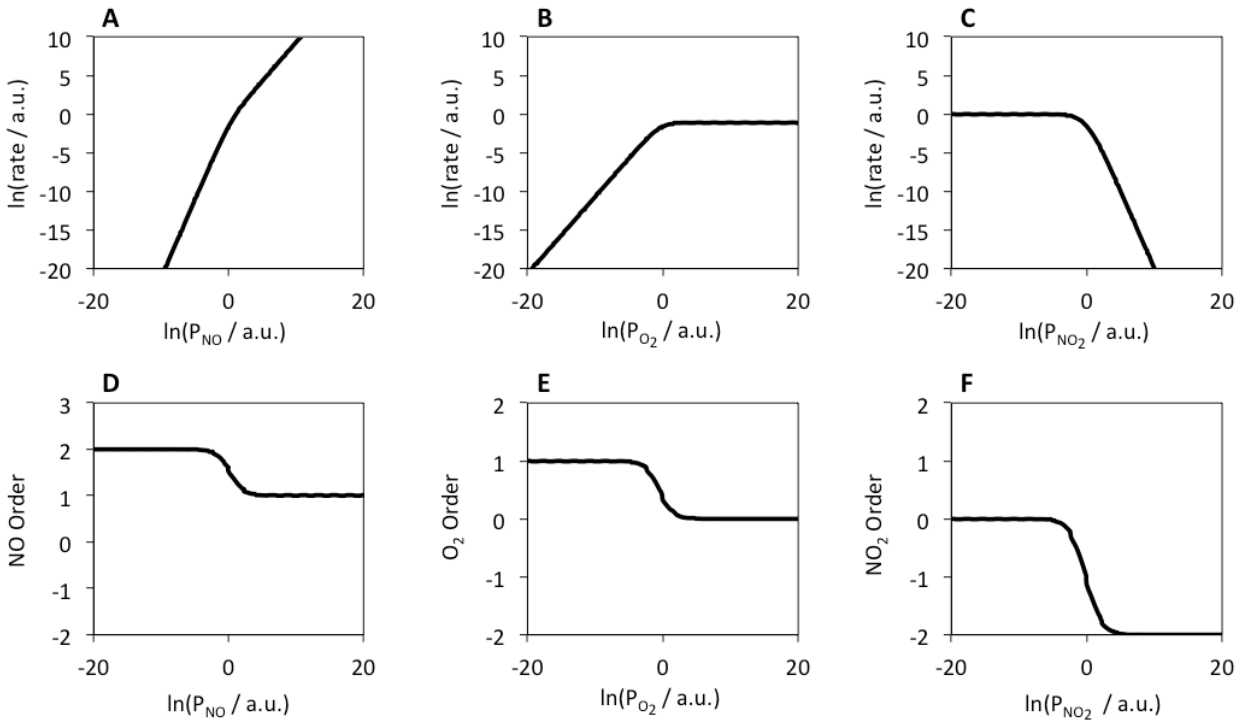

Figure S8. Effect of the (A) NO pressure, (B) O_2 pressure, and (C) NO_2 pressure on the NO oxidation rate and the NO, O_2, and NO_2 reaction orders (D, E, F, respectively) where the fourth elementary step of Scheme 1 is rate limiting. The NO order decreases from 2 to 1 with increasing NO pressure. The O_2 order decreases from 1 to 0 with increasing O_2 pressure. The NO_2 order decreases from 0 to -2 with increasing NO_2 pressure.

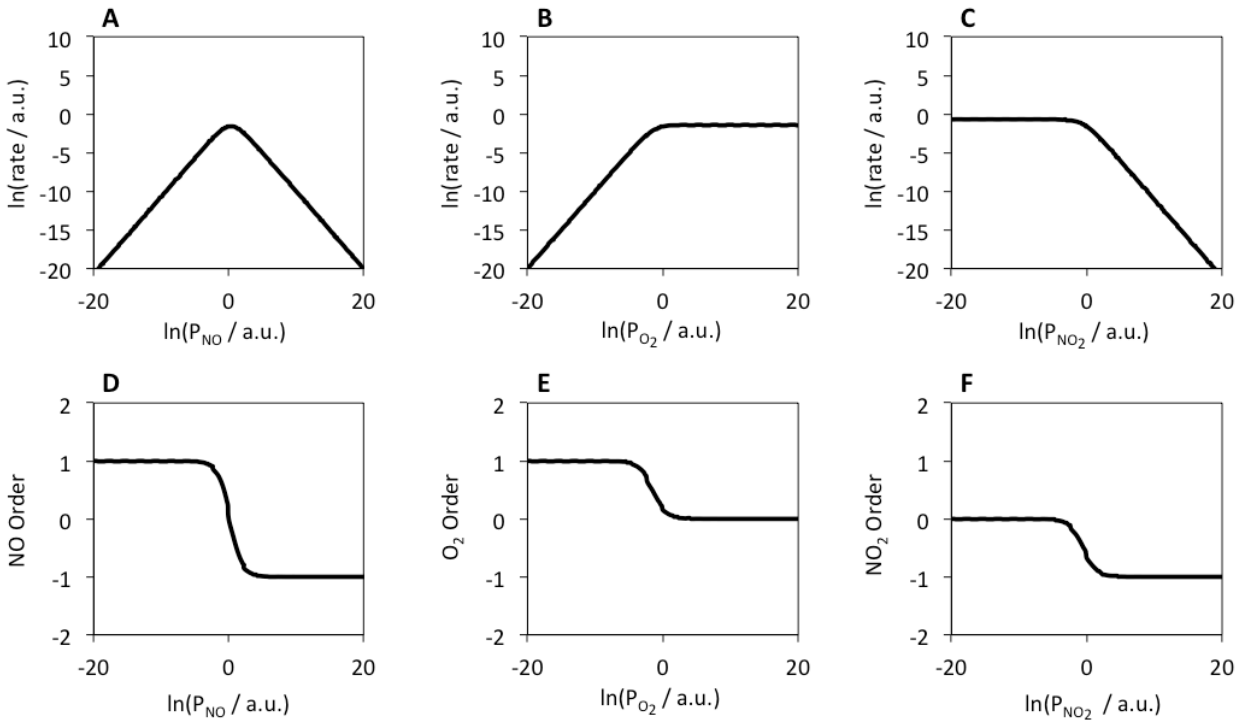

Figure S9. Effect of the (A) NO pressure, (B) O_2 pressure, and (C) NO_2 pressure on the NO oxidation rate and the NO, O_2, and NO_2 reaction orders (D, E, F, respectively) where the fifth elementary step of Scheme 1 is rate limiting. The NO order decreases from 1 to -1 with increasing NO pressure. The O_2 order decreases from 1 to 0 with increasing O_2 pressure. The NO_2 order decreases from 0 to -1 with increasing NO_2 pressure.

Section S7: References

[1] D.W. Fickel, R.F. Lobo, Copper Coordination in Cu-SSZ-13 and Cu-SSZ-16 Investigated by Variable-Temperature XRD, J. Phys. Chem. C. 114 (2010) 1633–1640. doi:10.1021/jp9105025.

[2] S.I. Zones, Zeolite SSZ-13 and its Method of Preparation, 4,544,538, 1985.

[3] U. Deka, A. Juhin, E. Eilertsen, H. Emerich, M.A. Green, S.T. Korhonen, B.M. Weckhuysen, A.M. Beale, Confirmation of Isolated Cu2+ Ions in SSZ-13 Zeolite as Active Sites in NH3-Selective Catalytic Reduction, J. Phys. Chem. C. 116 (2012) 4809–4818. doi:10.1021/jp212450d.

[4] A.J. Shih, J.M. González, I. Khurana, L.P. Ramírez, A. Peña L., A. Kumar, A.L. Villa, Influence of ZCuOH, Z2Cu, and Extraframework CuxOy Species in Cu-SSZ-13 on N2O Formation during the Selective Catalytic Reduction of NOx with NH3, ACS Catal. 11 (2021) 10362–10376. doi:10.1021/acscatal.1c01871.

[5] S.A. Bates, W.N. Delgass, F.H. Ribeiro, J.T. Miller, R. Gounder, Methods for NH3 titration of Brønsted acid sites in Cu-zeolites that catalyze the selective catalytic reduction of NOx with NH3, J. Catal. 312 (2014) 26–36. doi:10.1016/j.jcat.2013.12.020.

[6] J.R. Di Iorio, S.A. Bates, A.A. Verma, W.N. Delgass, F.H. Ribeiro, J.T. Miller, R. Gounder, The Dynamic Nature of Brønsted Acid Sites in Cu–Zeolites During NOx Selective Catalytic Reduction: Quantification by Gas-Phase Ammonia Titration, Top. Catal. 58 (2015) 424–434. doi:10.1007/s11244-015-0387-8.

[7] L.N. Wilcox, S.H. Krishna, C.B. Jones, R. Gounder, Mechanistic studies of NH3-assisted reduction of mononuclear Cu(II) cation sites in Cu-CHA zeolites, Catal. Sci. Technol. 11 (2021) 7932–7942. doi:10.1039/d1cy01646f.

[8] J.R. Di Iorio, R. Gounder, Controlling the Isolation and Pairing of Aluminum in Chabazite Zeolites Using Mixtures of Organic and Inorganic Structure-Directing Agents, Chem. Mater. 28 (2016) 2236–2247. doi:10.1021/acs.chemmater.6b00181.

[9] D.A. Hickman, J.C. Degenstein, F.H. Ribeiro, Fundamental principles of laboratory fixed bed reactor design, Curr. Opin. Chem. Eng. 13 (2016) 1–9. doi:10.1016/j.coche.2016.07.002.

[10] H.A. Massaldi, J.A. Maymo, Error in Handling Finite Conversion Reactor Data by the Differential Mehod, J. Catal. 14 (1969) 61–68. doi:10.1016/0021-9517(69)90356-X.

[11] F.H. Ribeiro, A.E. Schach von Wittenau, C.H. Bartholomew, G.A. Somorjai, Reproducibility of Turnover Rates in Heterogeneous Metal Catalysis: Compilation of Data and Guidelines for Data Analysis Reproducibility of Turnover Rates in Heterogeneous Metal Catalysis : Compilation of Data and Guidelines for Data Analysis, Catal. Rev. 39 (2006) 49–76. doi:10.1080/01614949708006468.

[12] H.S. Fogler, Essentials of Chemical Reaction Engineering, Pearson Education, 2010.

[13] V.J. Cybulskis, A.D. Smeltz, Y. Zvinevich, R. Gounder, W.N. Delgass, F.H. Ribeiro, Learning the fundamentals of kinetics and reaction engineering, Chem. Eng. Eduation. (2016) 202–210.

[14] J.W. Harris, A.A. Verma, J.W. Arvay, A.J. Shih, W.N. Delgass, F.H. Ribeiro, Consequences of Product Inhibition in the Quantification of Kinetic Parameters, J. Catal. 389 (2020) 468–475. doi:10.1016/j.jcat.2020.06.014.

[15] T. Beutel, J. Sarkany, G.-D. Lei, J.Y. Yan, W.M.H. Sachtler, J. Sa, Redox Chemistry of Cu/ZSM-5, J. Phys. Chem. 100 (1996) 845–851. doi:10.1021/jp952455u.

[16] P. Da Costa, B. Modén, G.D. Meitzner, D.K. Lee, E. Iglesia, Spectroscopic and chemical characterization of active and inactive Cu species in NO decomposition catalysts based on Cu-ZSM5, Phys. Chem. Chem. Phys. 4 (2002) 4590–4601. doi:10.1039/b203700a.

[17] D.K. Lee, Quantification and Redox Property of the Oxygen-Bridged Cu2+ Dimers as the Active Sites for the NO Decomposition over Cu-ZSM-5 Catalysts, Korean J. Chem. Eng. 21 (2004) 611–620. doi:10.1007/BF02705495.

[18] J. Wang, V.F. Kispersky, W. Nicholas Delgass, F.H. Ribeiro, Determination of the Au active site and surface active species via operando transmission FTIR and isotopic transient experiments on 2.3 wt.% Au/TiO 2 for the WGS reaction, J. Catal. 289 (2012) 171–178. doi:10.1016/j.jcat.2012.02.008.

[19] V.J. Cybulskis, J.W. Harris, Y. Zvinevich, A transmission infrared cell design for temperature-controlled adsorption and reactivity studies on heterogeneous catalysts, 103101 (2016). doi:10.1063/1.4963665.

[20] A.A. Verma, S.A. Bates, T. Anggara, C. Paolucci, A.A. Parekh, K. Kamasamudram, A. Yezerets, J.T. Miller, W.N. Delgass, W.F. Schneider, F.H. Ribeiro, NO oxidation: A probe reaction on Cu-SSZ-13, J. Catal. 312 (2014) 179–190. doi:10.1016/j.jcat.2014.01.017.

[21] B. Ipek, M.J. Wulfers, H. Kim, F. Göltl, I. Hermans, J.P. Smith, K.S. Booksh, C.M. Brown, R.F. Lobo, Formation of [Cu2O2]2+ and [Cu2O]2+ towards C–H Bond Activation in Cu-SSZ-13 and Cu-SSZ-39, ACS Catal. 7 (2017) 4291–4303. doi:10.1021/acscatal.6b03005.

[22] H. Li, C. Paolucci, I. Khurana, L.N. Wilcox, F. Göltl, J.D. Albarracin-Caballero, A.J. Shih, F.H. Ribeiro, R. Gounder, W.F. Schneider, Consequences of exchange-site heterogeneity and dynamics on the UV-visible spectrum of Cu-exchanged SSZ-13, Chem. Sci. 10 (2019) 2373–2384. doi:10.1039/c8sc05056b.